Arecibo HI absorption measurements of pulsars and the electron density at intermediate longitudes in the first galactic quadrant

J. M. Weisberg
Carleton College

S. Stanimirovic
University of California, Berkeley

K. Xilouris
University of Arizona

A. Hedden,
Carleton College

A. de la Fuente
Carleton College

THE ASTROPHYSICAL JOURNAL, 674:286–294, 2008 February 10

ARECIBO H I ABSORPTION MEASUREMENTS OF PULSARS AND THE ELECTRON DENSITY AT INTERMEDIATE LONGITUDES IN THE FIRST GALACTIC QUADRANT

J. M. WEISBERG,[1] S. STANIMIROVIĆ,[2] K. XILOURIS,[3] A. HEDDEN,[1,3]
A. DE LA FUENTE,[1] S. B. ANDERSON,[4] AND F. A. JENET[4,5]
Received 2007 January 6; accepted 2007 September 10

ABSTRACT

We have used the Arecibo telescope to measure the H I absorption spectra of eight pulsars. We show how kinematic distance measurements depend on the values of the Galactic constants R_0 and Θ_0, and we select our preferred current values from the literature. We then derive kinematic distances for the low-latitude pulsars in our sample and electron densities along their lines of sight. We combine these measurements with all others in the inner Galactic plane visible from Arecibo to study the electron density in this region. The electron density in the interarm range $48^\circ < l < 70^\circ$ is $0.017^{+0.012}_{-0.007}$(68% c.l.) cm^{-3}. This is $0.75^{+0.49}_{-0.22}$(68% c.l.) of the value calculated by the Galactic electron density model of Cordes & Lazio. The model agrees more closely with electron density measurements toward Arecibo pulsars lying closer to the Galactic center, at $30^\circ < l < 48^\circ$. Our analysis leads to the best current estimate of the distance of the relativistic binary pulsar B1913+16: $d = 9.0 \pm 3$ kpc. We use the high-latitude pulsars to search for small-scale structure in the interstellar hydrogen observed in absorption over multiple epochs. PSR B0301+19 exhibited significant changes in its absorption spectrum over 22 yr, indicating H I structure on a $\sim$500 AU scale.

Subject headings: Galaxy: fundamental parameters — ISM: abundances — ISM: clouds — ISM: structure — pulsars: general — radio lines: ISM

1. INTRODUCTION

Neutral hydrogen (H I) absorption measurements of pulsar signals at $\lambda = 21$ cm are important probes of various properties of the interstellar medium such as the small-scale structure of cold H I (Dickey et al. 1981; Stanimirović et al. 2003b) and calibrators of the pulsar distance scale and electron density models at large Galactic distances (Weisberg et al. 1979, 1987, 1995; Frail & Weisberg 1990). These measurements are complementary to interferometrically determined parallaxes, which can be utilized on nearer sources (Brisken et al. 2002; Chatterjee et al. 2004). We report new Arecibo[6] H I absorption observations of eight pulsars, and we use these measurements to study the electron density of the interstellar medium and the small-scale structure of neutral hydrogen clouds.

Sensitivity limitations indicate that few, if any, additional pulsar H I absorption measurements of electron density in the Galactic plane at the intermediate first-quadrant Galactic longitudes accessible to the Arecibo telescope will be made in the next decade or so. Hence, it is an appropriate time to combine the new results with all previous pulsar H I measurements at these longitudes to globally assess the density in the Galactic plane in this region. We use this information to estimate the distance to the relativistic binary pulsar B1913+16. In addition, H I absorption measurements on some of our high-latitude pulsars were originally measured over 20 years ago, during which interval the pulsars have moved many AU through the interstellar medium. Hence, comparison of the old and new absorption spectra yields information on the small-scale structure of the absorbing neutral hydrogen.

The plan of the paper is as follows: The pulsar H I absorption observational technique is sketched in the next section (§ 2). We present H I absorption spectra and kinematic distance results for low-latitude pulsars in § 3. In § 4 we use all measured pulsar distances in the inner Galactic plane visible from Arecibo Observatory to analyze the electron density in that region. In § 4.1 we review the latest work on the galactocentric distance of the Sun and the orbital velocity of the local standard of rest (LSR) in order to select an optimum model to use in refining pulsar kinematic distances and Galactic electron densities. Then in § 4.2 we apply the results of §§ 4 and 4.1 to determine the distance of the relativistic binary pulsar PSR B1913+16. We provide absorption spectra of high-latitude pulsars in § 5, along with analyses of the time variability of absorption in those cases in which earlier epoch data are available. Finally, we discuss our conclusions in § 6.

2. OBSERVATIONS

All observations were made with the 305 m Arecibo telescope from 1998 to 2000. The radio frequency signals near 1420 MHz were mixed to baseband, sampled, and recorded with the Caltech Baseband Recorder (CBR; Jenet et al. 2001), a 10 MHz bandwidth, fast-sampling receiver backend. Every 100 ns, the CBR sampled complex voltages with four-level digitization from the two orthogonally polarized feed channels, and recorded the samples to tape for later processing. (For additional details of the observing techniques and equipment, see Stanimirović et al. 2003a, 2003b.) The data were then corrected for quantization (Jenet & Anderson 1998), Fourier transformed, and folded modulo the apparent pulsar period with the supercomputers of Caltech's Center for Advanced Computing Research, resulting in data cubes consisting of intensity as a function of pulsar rotational phase (128 phase bins) and radio frequency (2048 frequency channels,

[1] Department of Physics and Astronomy, Carleton College, Northfield, MN 55057.
[2] Department of Astronomy, University of California, Berkeley, CA 94720.
[3] Department of Astronomy, University of Arizona, Tucson, AZ 85721.
[4] Department of Astronomy, California Institute of Technology, MS 105-24, Pasadena, CA 91125.
[5] Center for Gravitational Wave Astronomy, University of Texas, Brownsville, TX 78520.
[6] The Arecibo Observatory is part of the National Astronomy and Ionosphere Center, which is operated by Cornell University under a cooperative agreement with the National Science Foundation.

TABLE 1

Observing Parameters and Measured Kinematic Distances for Low-Latitude Pulsars

PSR J	PSR B	t_{obs} (hr)	$T_{sys,off\text{-}line}$ (K)	$\sigma_{\tau,off\text{-}line}$	l (deg)	b (deg)	DM (pc cm^{-3})	v_l[a] (km s^{-1})	v_u[a] (km s^{-1})	d_l[b] (km s^{-1})	d_u[b] (km s^{-1})
J1909+0254	B1907+02	3.0	45	0.11	37.6	−2.7	171.7	60	...	3.8 ± 0.5	...
J1922+2110	B1920+21	2.5	43	0.09	55.3	2.9	217.1	TP[c]	−65	4.8 ± 1.8	16.2 ± 1.0
J1926+1648	B1924+16	7.4	45	0.06	51.9	0.1	176.9	TP[c]	−47	5.2 ± 1.8	14.9 ± 0.8

[a] Here v_l and v_u are lower and upper velocity limits, respectively.

[b] Here d_l and d_u are lower and upper distance limits, respectively. A flat Fich et al. (1989) rotation curve with the standard IAU values of R_0 and Θ_0 (Kerr & Lynden-Bell 1986) was used.

[c] The tangent point velocity is adopted as the lower limit.

each having 1 km s^{-1} width). Subsequent processing at Carleton College collapsed the data cubes into two spectra: the pulsar-*on* spectrum is a sum of the spectra gathered during the pulsar pulse weighted by $I_{psr}(\phi)^2$, while the sum of those gathered in the interval between pulses is called the pulsar-*off* spectrum. Here $I_{psr}(\phi)$ is the broadband pulsar intensity in a given pulse phase bin ϕ.

Two final spectra are formed and displayed for each pulsar. The pulsar *absorption* spectrum, which represents the spectrum of the pulsar alone less any absorption caused by intervening neutral hydrogen, is the normalized difference of the pulsar-*on* and pulsar-*off* spectra. In order to maximize sensitivity, multiple integrations are summed with a weight depending on the square of the pulsar signal strength $I_{psr}(t)$ during each integration. In some cases, additional sensitivity was achieved by Hanning smoothing the final absorption spectrum, yielding a resolution of 2 km s^{-1}. (Any absorption spectrum that has been Hanning smoothed is labeled as such when displayed below.) The H I *emission* spectrum is the time-integrated, pulsar-*off* spectrum, calibrated in brightness temperature units by matching its peak with the Leiden/Argentine/Bonn H I Survey (Hartmann & Burton 1997, p. 243; Arnal et al. 2000; Bajaja et al. 2005; Kalberla et al. 2005). All spectra were frequency switched, and low-order polynomials were fitted to and removed from them in some cases in order to flatten intrinsic or scintillation-induced bandpass ripples.

The basic observing parameters are tabulated for low- and high-latitude pulsars in Tables 1 and 3, respectively. The quantities $T_{sys,off\text{-}line}$ and $\sigma_{\tau,off\text{-}line}$, the system temperature and measured 1 σ noise in optical depth away from the H I line, are both given. The former value is the sum of an estimated 40 K receiver contribution, plus a sky background determined by extrapolating the 408 MHz sky temperature (Haslam et al. 1982) at the pulsar position to 1420 MHz with a spectral index of −2.6. The H I emission line itself contributes significantly to the system temperature (and hence to the noise) at those velocities where it is present. To determine the expected optical depth noise at any velocity v, one may use $\sigma_\tau(v) = \sigma_{\tau,off\text{-}line} \times [T_{H\,I}(v) + T_{sys,off\text{-}line}]/T_{sys,off\text{-}line}$, where $T_{H\,I}(v)$ is the measured brightness temperature of H I at that velocity.

3. KINEMATIC DISTANCE ANALYSES AND RESULTS ON LOW-LATITUDE PULSARS

A low-latitude pulsar H I absorption spectrum can be used to set limits on the pulsar's distance, using the "kinematic" technique. A pulsar is farther than an H I cloud that absorbs its signal, and closer than one that does *not*. The latter "no absorption" criterion is impossible to ascertain in real spectra because of the inevitable presence of noise which could mask weak absorption. However, it was shown by Weisberg et al. (1979) that emission features with $T_b \geq 35$ K almost always exhibit significant absorption of radiation from background objects. Therefore, subsequent investigators have assigned an upper distance limit only at the velocity where one finds both no significant absorption, *and* an emission feature of $T_b \geq 35$ K. We use a flat Fich et al. (1989) Galactic rotation model and the IAU Galactic constants of $R_0 = 8.5$ kpc and $\Theta_0 = 220$ km s^{-1} (Kerr & Lynden-Bell 1986) to convert the radial velocities to distance. The resulting model radial velocities are shown in a panel under each absorption/emission spectrum pair. We also add and subtract velocities of 7 km s^{-1} to our nominal velocities, in order to derive estimates of the uncertainties in distance limits due to streaming and random gas motions in the Galaxy. These procedures are identical to those used in the critical evaluation of all such measurements then extant by Frail & Weisberg (1990) and by all subsequent pulsar H I absorption experimenters. Hence, our results are directly intercomparable with these earlier ones. Our derived distance limits are discussed below for each pulsar, and are summarized in Table 1. See § 4.1 for a discussion of modifications to our derived distances for different values of the Galactic constants.

3.1. *PSR J1909+0254=B1907+02 (l=37.6°; b=−2.7°), Fig. 1*

The farthest observed absorption feature is at $v = 60$ km s^{-1}, well before the tangent point. Hence, the pulsar lies beyond a

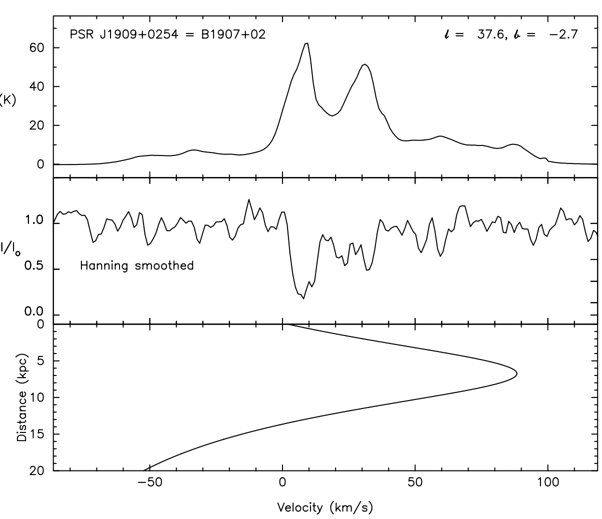

Fig. 1.—For PSR J1909+0254 = B1907+02. *Top*: H I emission spectrum in the direction of the pulsar. *Middle*: Pulsar absorption spectrum. The resolution is 1 km s^{-1} unless Hanning smoothing is indicated, in which case it is 2 km s^{-1}. *Bottom*: Radial velocity as a function of distance, calculated from a Fich et al. (1989) flat rotation curve with the standard IAU values of R_0 and Θ_0 (Kerr & Lynden-Bell 1986). See text for procedures to determine distances with other choices of R_0 and Θ_0.

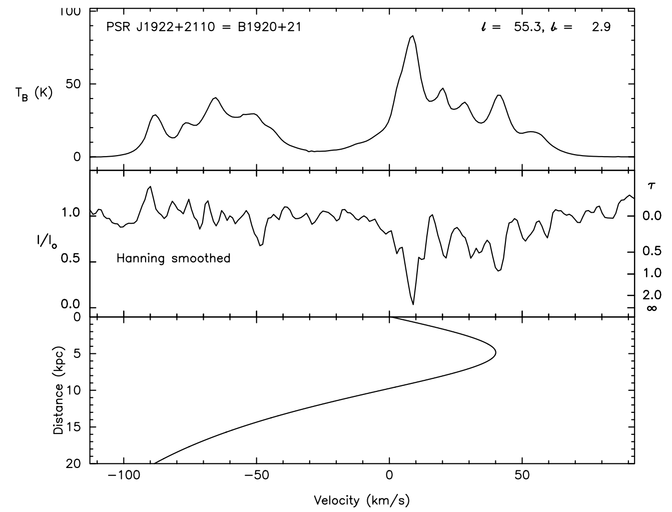

FIG. 2.—Same as Fig. 1, but toward PSR J1922+2110 = B1920+21.

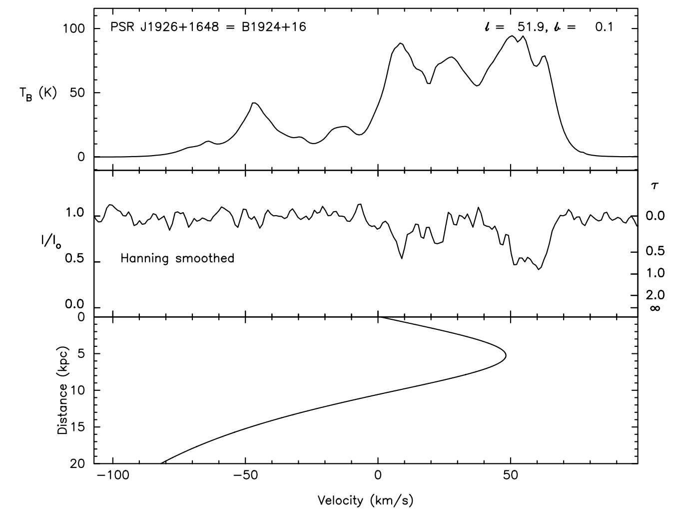

FIG. 3.—Same as Fig. 1, but toward PSR J1926+1648 = B1924+16.

lower distance limit of 3.8 ± 0.5 kpc. Unfortunately, the H I emission has $T_b \lesssim 10$ K at all velocities where one might test for an upper distance limit via lack of absorption, because the $b = 2.7°$ line of sight rapidly leaves the hydrogen layer. Since significant absorption could not in any case be guaranteed at the velocity of such weak emission (Weisberg et al. 1979), no upper distance limit can be set.

3.2. *PSR J1922+2110=B1920+21 (l=55.3°; b=2.9°), Fig. 2*

Weisberg et al. (1987) observed this pulsar. Their H I spectrum was contaminated by interstellar scintillation and was rather noisy, prompting us to reobserve it with greater sensitivity. The highest velocity absorption that Weisberg et al. (1987) could confidently detect was at $v = 26$ km s^{-1}, leading to their limit of 1.9 ± 0.7 kpc $\lesssim d$. Our new observations clearly exhibit absorption at $v = 41$ km s^{-1}, near the tangent point. Hence, we revise the lower distance limit significantly upward: 4.8 ± 1.8 kpc $\lesssim d$. The Weisberg et al. (1987) spectrum also showed an absorption feature at this velocity, but it was not sufficiently above the noise to serve as a reliable kinematic distance indicator. The dip in the current absorption spectrum at $v = -48$ km s^{-1} is probably noise and will not be used to set a distance limit. (It appears much more prominently in one of the two circular polarization channels than in the other, and is not visible in the Weisberg et al. [1987] absorption spectrum. Furthermore, the nearby source G55.6+2.3 = B1923+210 does not exhibit reliable far-side absorption until $v \lesssim -60$ km s^{-1} [Dickey et al. 1983; Colgan et al. 1988].) Conversely, the *lack* of absorption in the $T_b = 41$ K emission feature at $v = -65$ km s^{-1} sets the upper distance limit of $d \lesssim 16.2 \pm 1.0$ pc.

3.3. *PSR J1926+1648=B1924+16 (l=51.9°; b=0.1°), Fig. 3*

While the Fich et al. (1989) model predicts a tangent point velocity of 48 km s^{-1} in this direction, we detect significant emission and absorption well beyond this velocity, with the last major feature centered near $v = 61$ km s^{-1}. These features are due to the Sagittarius arm (Burton 1970). Garwood & Dickey (1989) and Colgan et al. (1988) also observe H I absorption out to these velocities in the nearby sources G50.625−0.031 and G51.4−0.0, respectively. We choose the tangent point as our lower distance limit, so 5.2 ± 1.8 kpc $\lesssim d$. The lack of absorption in the $T_b \sim 42$ K emission feature at $v \sim -47$ km s^{-1} yields the upper distance limit: $d \lesssim 14.9 \pm 0.8$ kpc.

4. ANALYSIS OF THE ELECTRON DENSITY IN THE INNER GALACTIC PLANE VISIBLE FROM ARECIBO

The currently reported H I absorption distance measurements are probably among the last to be determined at Arecibo in the foreseeable future, as all known pulsars having sufficient flux density to achieve adequate S/N in a reasonable time have now been measured as well as is possible with this procedure. Unfortunately, Galactic H I emission is now the dominant noise source, so that future receiver improvements will not significantly decrease the overall noise. Therefore, new low-latitude pulsars discovered in the future in this longitude range will probably be too faint for the H I absorption technique, even at Arecibo. Consequently, now is a good time to review all such measurements and their implications for the electron density in the inner Galactic plane visible from Arecibo.

The dispersion measure DM of a pulsar, derived from multiple-frequency timing measurements and reported in Manchester et al. (2005),[7] directly yields the path-integrated electron density along the line of sight: DM $= \int n_e\, ds$. Hence, our distance limits, d, can be combined with the published dispersion measures to yield mean electron densities $\langle n_e \rangle$ along the line of sight:

$$\langle n_e \rangle \equiv \frac{\int n_e\, ds}{d} = \frac{\mathrm{DM}}{d}. \quad (1)$$

Table 2 lists the electron density limits derived in this fashion from our measurements and from all earlier ones in similar directions; i.e., toward the inner Galactic plane accessible to the Arecibo telescope. Note that the kinematic distances listed in Table 2 were all derived with the standard procedures discussed above in § 3, namely, the uniform criteria established by Frail & Weisberg (1990) and the IAU standard Galactic constants (Kerr & Lynden-Bell 1986). Procedures to modify these values for other choices of Galactic constants are given below in § 4.1.

In Figure 4*a* we display measured limits on the mean electron density as a function of Galactic longitude l in the inner Galactic plane visible from Arecibo. Only those pulsars from Table 2 with $|b| < 3°$ and a lower distance limit $d_l \geq 1$ kpc are included in

[7] The catalog is maintained and updated at http://www.atnf.csiro.au/research/pulsar/psrcat.

TABLE 2

Measured Electron Densities toward Pulsars with $30^\circ < l < 70^\circ$, $|b| < 3^\circ$, and 1 kpc $\leq d$

PSR J	PSR B	l (deg)	b (deg)	DM (pc cm^{-3})	d_l[a] (kpc)	d_u[a] (kpc)	$\langle n_{e,u}\rangle$[b] (cm^{-3})	$\langle n_{e,l}\rangle$[b] (cm^{-3})	Distance Ref.[c]	Assoc.
J1848−0123	B1845−01	31.34	0.04	159.5	4.2	4.8	0.038	0.033	FW90	
J1852+0031	B1849+00	33.52	0.02	787.0	7.1	16.6	0.111	0.047	FW90	
J1856+0113	B1853+01	34.56	−0.50	96.7	2.7	3.9	0.036	0.025	C75	SNR: W44
J1857+0212	B1855+02	35.62	−0.39	506.8	6.9		0.073		FW90	
J1901+0331	B1859+03	37.21	−0.64	402.1	6.8	15.1	0.059	0.027	FW90	
J1901+0716	B1859+07	40.57	1.06	252.8	2.8	4.7	0.090	0.054	FW90	
J1902+0556	B1900+05	39.50	0.21	177.5	3.1	4.3	0.057	0.041	FW90	
J1902+0615	B1900+06	39.81	0.34	502.9	6.5	15.8	0.077	0.032	FW90	
J1903+0135	B1900+01	35.73	−1.96	245.2	2.8	4.0	0.088	0.061	FW90	
J1905+0154A		36.20	−2.20	194.0	6.4	8.2	0.030	0.024	R97	GC: NGC 6749
J1906+0641	B1904+06	40.60	−0.30	472.8	6.5	14.0	0.073	0.034	FW90	
J1909+0254	B1907+02	37.60	−2.71	171.7	3.8		0.045		This work	
J1909+1102	B1907+10	44.83	0.99	150.0	4.3	6.0	0.035	0.025	FW90	
J1915+1009	B1913+10	44.71	−0.65	241.7	6.0	14.5	0.040	0.017	FW90	
J1916+1312	B1914+13	47.58	0.45	237.0	4.0	5.7	0.059	0.042	FW90	
J1917+1353	B1915+13	48.26	0.62	94.5	4.8	5.7	0.020	0.017	FW90	
J1922+2110	B1920+21	55.28	2.93	217.1	4.8	16.2	0.045	0.013	This work	
J1926+1648	B1924+16	51.86	0.06	176.9	5.2	14.9	0.034	0.012	This work	
J1930+1852		54.10	0.27	308.0	3.2[d]	10[d]	0.096	0.031	VB88; LAS01	SNR: G54.1+ 0.3
J1932+2020	B1929+20	55.57	0.64	211.2	4.8	14.9	0.044	0.014	FW90	
J1932+2220	B1930+22	57.36	1.55	219.2	10.4	13.7	0.021	0.016	FW90	
J1935+1616	B1933+16	52.44	−2.09	158.5	5.2		0.030		FW90	
J1939+2134	B1937+21	57.51	−0.29	71.0	4.6	14.8	0.015	0.005	FW90	
J1952+3252	B1951+32	68.77	2.82	45.0	1.0	4.0	0.045	0.011	B84	SNR: CTB80
J2004+3137	B2002+31	69.01	0.02	234.8	7.0	12.0	0.034	0.020	FW90	

[a] Here d_l and d_u are lower and upper distance limits, respectively. A flat Fich et al. (1989) rotation curve with the standard IAU values of R_0 and Θ_0 (Kerr & Lynden-Bell 1986) was used. See text for procedures to determine distances with other choices of R_0 and Θ_0.

[b] Here $\langle n_{e,u}\rangle$ and $\langle n_{e,l}\rangle$ are upper and lower mean electron density limits, respectively.

[c] Subsequent work by Lu et al. (2002) suggests $d \sim 5$ kpc under an assumption of uniform H I density in this direction, which the present authors find unlikely. (See Fig. 5.)

References.—B84, Blair et al. 1984; C75, Caswell et al. 1975; FW90, Frail & Weisberg 1990; LAS01, Lu et al. 2001; R97, Rosino et al. 1997; VB88, Velusamy & Becker 1988. Other data are from the ATNF Pulsar Catalogue at http://www.atnf.csiro.au/research/pulsar/psrcat (Manchester et al. 2005).

Figure 4*a* in order to concentrate on kiloparsec-scale averages in the Galactic plane. Almost all of these measurements were derived from Arecibo pulsar H I absorption spectra. While there is significant scatter, it is apparent that the measured densities tend to decline as the line of sight rotates away from the inner Galaxy, with a notable drop in the region between the Sagittarius arm (the first arm interior to our location) and the local spiral arm (see Fig. 5). Ables & Manchester (1976) were the first to have adequate $\langle n_e\rangle$ measurements to infer that interarm densities are lower than those in spiral arms. As illustrated in Figure 4*a*, the numerous measurements made since that epoch serve to confirm and refine their suggestion, at least in this particular interarm region. Indeed, the drop in $\langle n_e\rangle$ as l exceeds 48° corresponds with the line of sight finally reaching a longitude at which it no longer intercepts the Sagittarius arm (see Fig. 5). Meanwhile, with only one exception, *every* pulsar measurement in the interarm range $48^\circ < l < 70^\circ$ is consistent with a relatively low $\langle n_e\rangle \sim 0.02$ cm^{-3} (see below for further analysis). The electron density at lower latitudes sampled in Figure 4*a* is clearly significantly higher, with an average in the vicinity of 0.05 cm^{-3} (plus superposed variations) in the 30°–40° longitude range.

It is also useful to compare our updated set of electron density measurements with the most widely used Galactic density model (NE2001; Cordes & Lazio 2002). Figure 4*b* exhibits the measured limits on $\langle n_e\rangle$, normalized by the mean electron densities *predicted* by the NE2001 model. The measured-to-model electron density ratio hovers near 1 (with some inevitable scatter) for $l \lesssim 48^\circ$, indicating that the model fits the data adequately at those longitudes. However, at the higher longitudes $48^\circ < l < 70^\circ$ discussed above, there is a tendency for the typical measured-to-model density ratio to lie below 1, suggesting that the NE2001 model densities are somewhat high in this interarm region.

In order to further explore the electron density in this interarm region, we performed Monte Carlo simulations to assess the best value and uncertainty on $\langle n_e\rangle$ and on the measured-to-model $\langle n_e\rangle$ ratio for the pulsars in this region. Of the 10 pulsars with measured distance limits and limits on $\langle n_e\rangle$ in this range (see Table 2), we discarded the data from PSR J1935+1616, since it lacks a measured upper distance and lower density limit. For each of the remaining nine pulsars, all possible distances between the measured upper and lower limits were rendered equally probable in our simulations by choosing distances randomly from a uniform distribution between the measured distance limits. Note that the assumption of uniform probability is the simplest reasonable hypothesis for measurements such as these which have only a lower and upper limit. We find that $\langle n_e\rangle = 0.017^{+0.012}_{-0.007}$ (68% c.l.) cm^{-3}, and that the ratio of measured-to-NE2001 electron density is $0.75^{+0.49}_{-0.22}$ (68% c.l.) for $48^\circ < l < 70^\circ$. Future models should take this discrepancy into account.

For simplicity, both the measured and model densities discussed above are based on the standard IAU Galactic constants. As described below in § 4.1, the *ratio* plotted in Figure 4*b* remains virtually identical if both constituents are rescaled to incorporate other choices of Galactic constants.

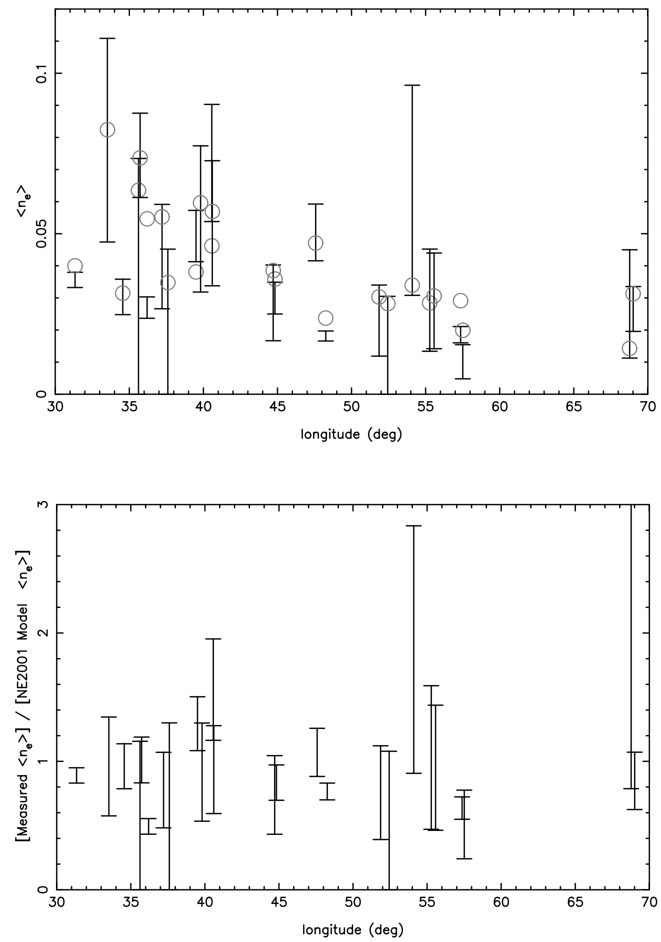

FIG. 4.—Mean electron density in the inner Galactic plane visible from Arecibo Observatory. The IAU (Kerr & Lynden-Bell 1986) values of R_0 and Θ_0 were used; see text for procedures to rescale with other values. Pulsars in Table 2 with $d_l < 1$ kpc or $|b| > 3°$ are not shown. *Top*: Measured electron density limits (*error bars*) and NE2001 model electron densities (*circles*) vs. longitude. *Bottom*: Ratio of measured electron density to the NE2001 model value, vs. longitude.

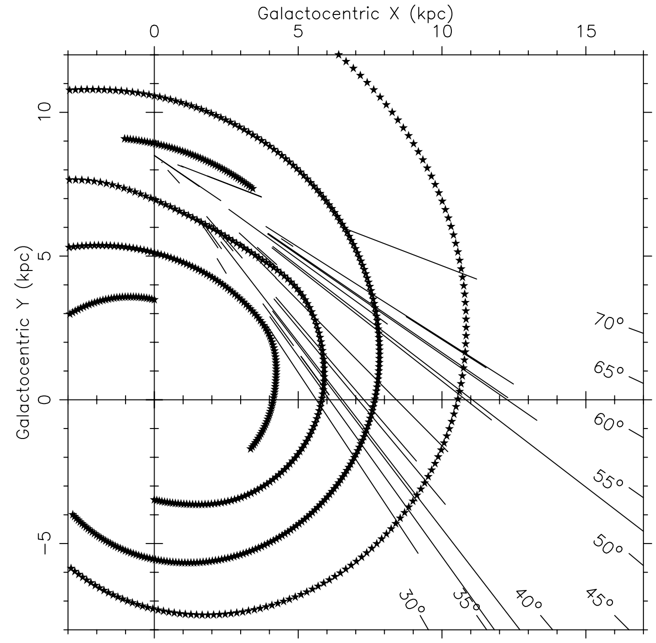

FIG. 5.—Galactic plane, showing spiral arms (Cordes & Lazio 2002) and Arecibo inner Galactic plane pulsars with measured distances [upper and lower limits are delineated by the ends of lines pointing at the Sun, which is at $(X, Y) = (0.0, 8.5)$ kpc]. Galactic longitudes in the Arecibo range, $30° \le l \le 70°$, are shown at the bottom and right edges of the plot. Note especially the long interarm path in the direction of PSR B1913+16, at $l \sim 50°$.

4.1. *The Effects of Improved Galactic Constants R_0 and Θ_0*

Much progress has been made on Galactic structure and kinematics in the ~20 years since the IAU constants were defined. Therefore, it is useful to discuss improved measurements of R_0 and Θ_0, and to investigate the influence of these better values on the kinematic distances and electron densities discussed in §§ 3 and 4.

From remarkable proper motion and radial velocity measurements of the orbit of star S2 about Sgr A* through much of its 15 yr period, Eisenhauer et al. (2005) find that the distance to the Galactic center $R_0 = 7.62 \pm 0.32$ kpc. Reid & Brunthaler (2004) have made equally stunning interferometric measurements of the proper motion of Sgr A*, which yield an angular velocity of the LSR about the Galactic center, $\Omega_0 = \Theta_0/R_0 = (29.45 \pm 0.15)$ km s^{-1} kpc^{-1}. Both of these measurements are notable in that they rest on far fewer assumptions than earlier determinations, and hence should be freer of systematic errors. Consequently, we adopt them in what follows. An even newer estimate of R_0 from infrared measurements of red clump giants in the Galactic bulge (Nishiyama et al. 2006) yields a value of 7.52 ± 0.10 (statistical) ± 0.35 (systematic) kpc, which is consistent with our above adopted value.

Consider material traversing a circular orbit in the plane at galactocentric radius R. Given a flat rotation curve with circular velocity Θ_0, its radial velocity with respect to the LSR is $v_{\rm rad} = \Theta_0(R_0/R - 1)\sin l$. With $R = (R_0^2 + d^2 - 2R_0 d \cos l)^{1/2}$, the distance as a function of $v_{\rm rad}$ is given by

$$d = R_0\left(\cos l \pm \sqrt{1 + \frac{v_{\rm rad}}{\Theta_0 \sin l} - \sin^2 l}\right). \quad (2)$$

Hence, our new adopted Galactic parameters, giving a small change in Θ_0 but a relatively large change in R_0, result in a recalibration of the distance in a particular direction, accomplished by rescaling it with an approximately constant factor of $R_{0,\rm new}/R_{0,\rm old} = 7.62/8.50 = 0.896$. Kinematic distance limits and Galactic distance models that use the old IAU Galactic constants should be adjusted by this factor to reflect the improved constants.

Figure 6 displays distance—radial velocity curves toward $l = 50°$ derived with the old and new flat Galactic rotation curves. Figure 6*a* illustrates that the old and new model distances differ primarily by a constant multiplicative factor, as indicated in the previous analysis. It follows from the above that when distance is *normalized* by R_0, the old and new radial velocity—distance curves are almost identical (Fig. 6*b*). Such normalized distances are useful in the analysis of the acceleration of pulsars in the Galactic gravitational field, as is discussed in the next section (§ 4.2).

As described above, the new Galactic constants would result primarily in the measured distances being rescaled by the ratio of new to old R_0. The electron densities, including model densities that have been calibrated via pulsar kinematic distance measurements, would then be rescaled by the inverse of this ratio (see eq. [1]). Hence, Figure 4*a* would be thus rescaled; while Figure 4*b* would remain unchanged, since it displays the ratio of two densities, each of which should be rescaled by the same factor.

4.2. *The Distance to the Relativistic Binary Pulsar B1913+16*

The relativistic binary pulsar B1913+16 lies in the heart of the region of the Galaxy that we are studying, at $(l, b) \sim (50°, 2°)$.

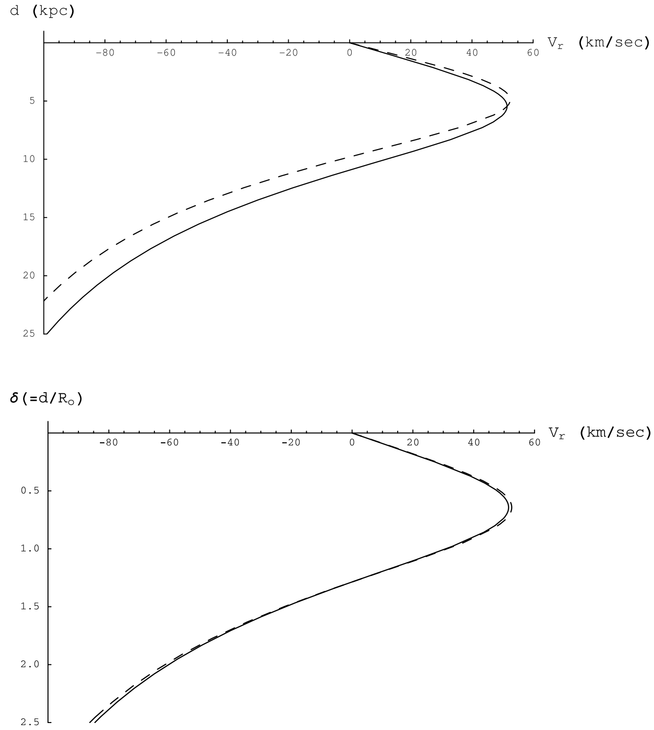

FIG. 6.—Calculated radial velocity as a function of distance along a line of sight in the Galactic plane at $l = 50°$. A flat rotation curve with the IAU (Kerr & Lynden-Bell 1986) values of R_0 and Θ_0 yields the solid line, while a flat rotation curve with new Galactic constants (see text) is shown by the dashed line. *Top*: Radial velocity vs. distance d along the line of sight. *Bottom*: Radial velocity vs. *normalized* distance δ along the line of sight, where $\delta = d/R_0$.

The orbital decay of this system due to gravitational wave emission provides a strong test of relativistic gravitation (Taylor & Weisberg 1989). Currently, the precision of the relativistic test is limited by uncertainties in the Galactic acceleration of the pulsar and the solar system (Damour & Taylor 1991), which are currently dominated by uncertainties in the pulsar distance d (or, more specifically, uncertainties in δ, the distance normalized by R_0 [Weisberg & Taylor 2003, 2005]). Hence, it is very important to assess the current results in an effort to improve our knowledge of B1913+16's distance.

Figure 4*a* shows that the measured electron density appears to have a local minimum near the pulsar's longitude. The relatively low value of $\langle n_e \rangle$ at $l \sim 50°$ is not surprising, since we noted in § 4 that the line of sight in this direction traverses a long path *between* spiral arms (see Fig. 5). The tightest limits on $\langle n_e \rangle$ in the whole inner plane visible from Arecibo are for PSR B1915+13 at $l = 48°$, which happens also to be the pulsar closest to PSR B1913+16. Hence, we adopt the measured limits from B1915+13, including an allowance for up to 7 km s^{-1} noncircular velocities (not shown in Table 2 or Fig. 4): $\langle n_e \rangle \sim (0.0188 \pm 0.006) \times (8.5\ \mathrm{kpc}/R_0)\ \mathrm{cm}^{-3}$. Note that this value is congruent with and has modestly tighter limits than the electron density derived in this interarm region in § 4.

Armed with our new estimate of $\langle n_e \rangle$, we use equation (1) to find the distance to PSR B1913+16, which has DM $\sim$ 169 pc cm^{-3}:

$$d_{\mathrm{B1913+16}} = (10.0 \pm 3.2)\left(\frac{R_0}{8.5\ \mathrm{kpc}}\right)\ \mathrm{kpc}. \quad (3)$$

Our result can also be compared with the Cordes & Lazio (2002) NE2001 model distance of $5.90(R_0/8.5\ \mathrm{kpc})$ kpc, which is lower for the reasons discussed above. Damour & Taylor (1991) used techniques similar to ours to estimate that $d_{\mathrm{B1913+16}} = (9.2 \pm 1.4)(R_0/8.5\ \mathrm{kpc})$. While the error bars of their and our estimates overlap significantly, we are not able to justify tightening them to the degree that Damour & Taylor (1991) did. Finally, adopting what we judged in § 4.1 to be the current best measurement of R_0 ($R_0 = 7.62 \pm 0.32$ kpc; Eisenhauer et al. 2005) leads to our best estimate of the distance to PSR B1913+16: $d_{\mathrm{B1913+16}} = 9.0 \pm 3$ kpc.

As noted above, the uncertainty in the general relativistic orbital decay rate of this pulsar is currently dominated by the uncertainty in the quantity $\delta_{\mathrm{B1913+16}}$. For these purposes, it is useful to give

$$\delta_{\mathrm{B1913+16}} \equiv d_{\mathrm{B1913+16}}/R_0 = 1.18 \pm 0.38. \quad (4)$$

5. HIGH GALACTIC LATITUDE PULSARS AND SEARCHES FOR TEMPORAL VARIABILITY OF ABSORPTION

Relatively nearby pulsars are excellent targets for studies of the tiny-scale atomic structure (Heiles 1997). Comparison of their H I absorption spectra at multiple epochs as they move across the sky permits us to study structure down to AU scales. We discuss here our measurements of five such pulsars. All but two have been previously observed, so we search for changes between the previous and current epochs. The pulsars' observing parameters, distances, and transverse velocities are listed in Table 3.

The pulsars discussed in this section are all located at high Galactic latitudes (in all cases, $|b| > 25°$). Since their lines of sight leave the Galactic hydrogen layer fairly quickly, they are not amenable to the kinematic distance technique discussed in § 3. Conversely, we cannot search for temporal absorption variations in the low-latitude pulsars of § 3 because two have never before

TABLE 3

OBSERVING PARAMETERS, ESTIMATED DISTANCES, AND TRANSVERSE SPEEDS OF HIGH-LATITUDE PULSARS

PSR J	PSR B	t_{obs} (hr)	$T_{\mathrm{sys,off\text{-}line}}$ (K)	$\sigma_{\tau,\mathrm{off\text{-}line}}$	DM (pc cm^{-3})	d [a] (kpc)	μ_{tot} [b] (mas yr^{-1})	Prop. Mo. Ref.	v_{trans} (AU yr^{-1})	v_{trans} (km s^{-1})
J0304+1932	B0301+19	1.3	41	0.015	15.737	0.62	37 (5)	LAS82	23	110
J1239+2453	B1237+25	1.4	41	0.009	9.242	0.85	115.6 (12)	B03	98	470
J1537+1155	B1534+12	1.7	42	0.13	11.61436	1.02	25.086 (20)	KWS03	26	121
J1543+0929	B1541+09	2.9	42	0.03	35.24	3.49	8.3 (10)	B03	29	140
J2305+3100	B2303+30	1.2	41	0.07	49.544	3.66	20 (2)	B03	73	350

[a] Distance d is from the DM and the Cordes & Lazio (2002) electron density model, except for J1239+2453 (interferometric parallax; Brisken et al. 2002) and J1537+1155 (differential galactic acceleration [see text]; Stairs et al. 2002).

[b] The uncertainty in units of the last digit of the quoted value is given in parentheses.

REFERENCES.—B03, Brisken et al. 2003; KWS03, Konacki et al. 2003; LAS82, Lyne et al. 1982. Other data are from the ATNF Pulsar Catalogue at http://www.atnf.csiro.au/research/pulsar/psrcat (Manchester et al. 2005).

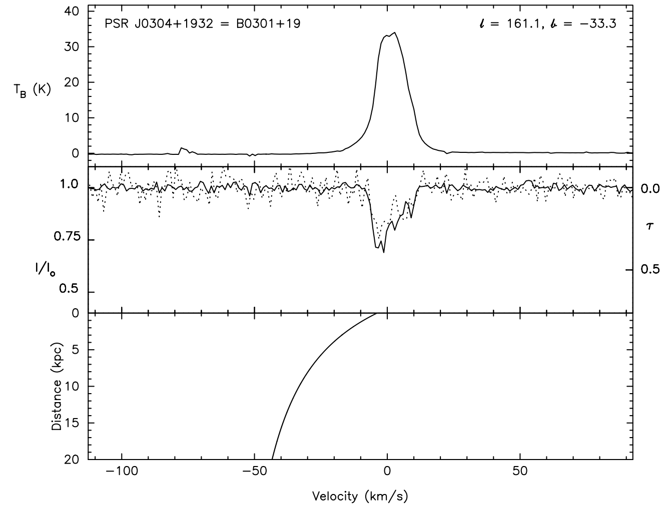

FIG. 7.—H I emission and pulsar absorption spectra, and rotation curve, toward PSR J0304+1932 = B0301+19. The 1976–1977 absorption spectrum of Dickey et al. (1981) is also plotted atop ours as a dotted line. Note that the absorption spectrum vertical scale is magnified for clarity. See the caption to Fig. 1 for additional details.

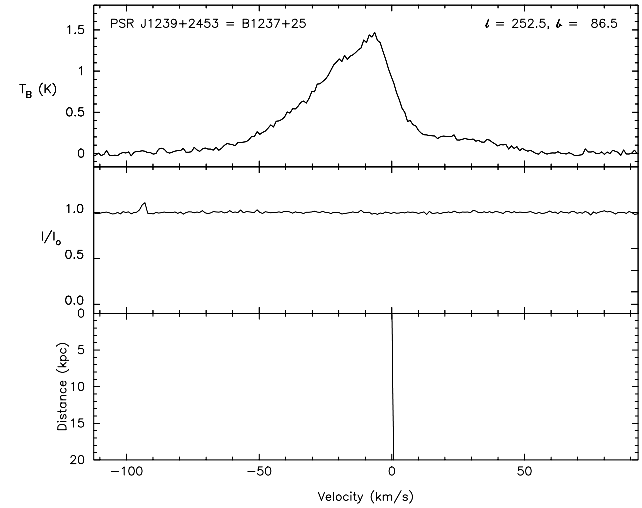

FIG. 9.—Same as Fig. 1, but toward PSR J1239+2453 = B1237+25.

been observed, and the third's absorption spectrum was too noisy at the earlier epoch to yield meaningful differences. (Indeed, we reobserved it in order to more confidently measure its kinematic distance because the noise in the earlier spectrum precluded a secure result.)

5.1. *J0304+1932=B0301+19* (*l=161.1°; b=−33.3°*), *Figs. 7 and 8*

The H I absorption spectrum of this pulsar was first observed in 1976–1977 by Dickey et al. (1981). That spectrum and our new one are plotted together in Figure 7. Both epochs' spectra have a similar $\sim$1 km s^{-1} resolution. Both the *integrated* optical depth (the equivalent width) and the depth of most individual absorption components have changed significantly between the two epochs. Although the early observations were gathered with a spectrometer that digitized the signal to only one bit, its response to rapidly varying pulsar signals was very well characterized by Weisberg (1978). Careful quantization corrections have also been made for the current epoch (Jenet & Anderson 1998). Hence, we believe that both spectra are accurate and that the change is real.

The channel spacing of the old and new spectra are 1.056 and 1.031 km s^{-1}, respectively. In order to study the absorption changes more carefully, we slightly coarsened the spacing of the new data via interpolation to match the channel spacing and center frequency of the old data. We also ensured that the old and new channel frequencies matched by verifying that the (essentially noise-free) *emission* spectra were consistent to less than a channel width. Figure 8 displays the old and (resampled) new absorption spectra (*top*) and their difference (*bottom*). The difference spectrum also displays a $\pm 2\,\sigma$ noise envelope in order to assess the significance of variations. (The noise envelope grows at the central velocities because the H I emission line itself contributes significantly to the system noise [Johnston et al. 2003; Stanimirović et al. 2003b].) The difference spectrum clearly shows a general trend whereby the absorption line depth is greater at the later epoch in most of the central channels, with the largest single-channel difference being significant at the 2.6 σ level.

The $\sim$22 yr time baseline is unique in being one of the longest extant showing absorption variations, leading to a length scale of $\sim$500 AU, which is second only to the PSR 1557−50 scale of

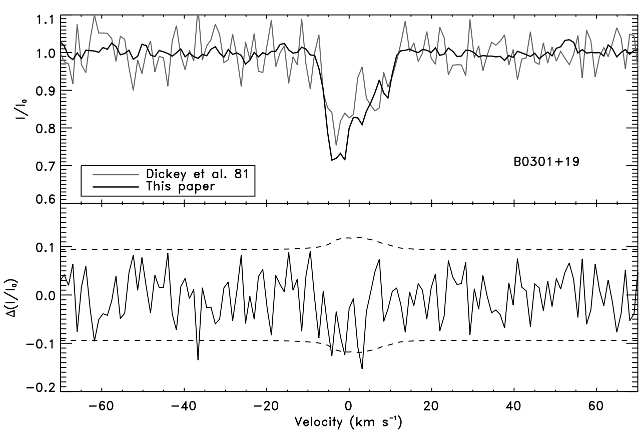

FIG. 8.—Changes in the absorption spectrum of PSR J0304+1932 = B0301+19 over 22 yr. *Top*: The old and new spectra are shown after the new spectrum has been interpolated to the same frequencies as the old spectra. This plot is similar to the middle panel of Fig. 7, except that the new spectrum in the earlier figure was not resampled. *Bottom*: The difference spectrum, with a $\pm 2\,\sigma$ error envelope superposed (*dashed lines*).

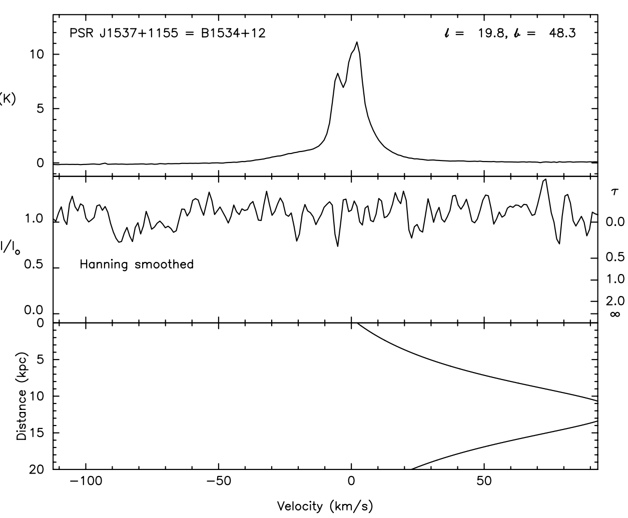

FIG. 10.—Same as Fig. 1, but toward PSR J1537+1155 = B1534+12.

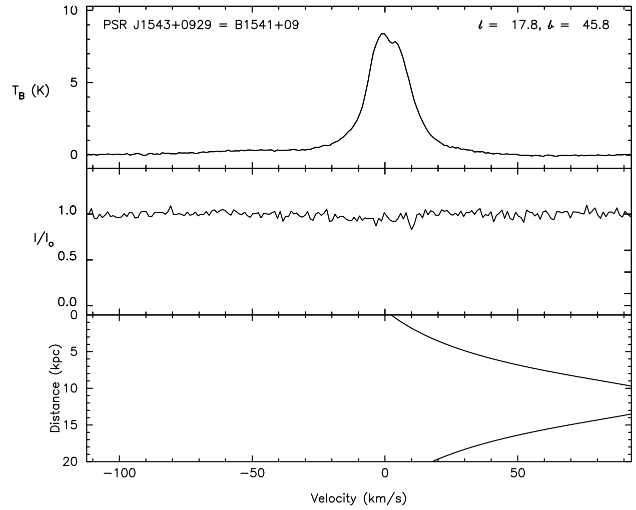

FIG. 11.—Same as Fig. 1, but toward PSR J1543+0929 = B1541+09.

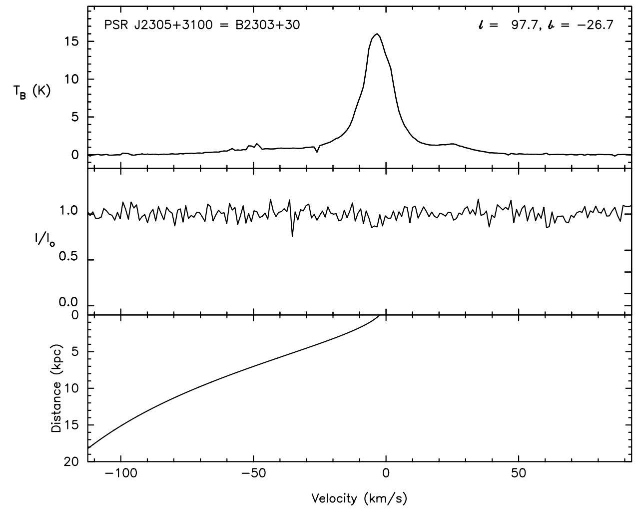

FIG. 12.—Same as Fig. 1, but toward PSR J2305+3100 = B2303+30.

$\sim$1000 AU (Johnston et al. 2003). Further implications of these results for small-scale structure in the interstellar medium will be analyzed in a separate paper (S. Stanimirović et al. 2008, in preparation).

5.2. *J1239+2453=B1237+25* (*l*=252.5°; *b*=86.5°), *Fig. 9*

Dickey et al. (1981) also measured the H I absorption spectrum of this pulsar in 1976–1977. The original and current pulsar spectra show no absorption. These results are not surprising, given the Galactic polar line of sight and the very weak H I emission in this direction. The pulsar moved $\sim$2200 AU between the two observations.

5.3. *J1537+1155=B1534+12* (*l*=19.8°; *b*=48.3°), *Fig. 10*

This pulsar is a member of a double neutron star binary system. Its pulse timing parallax gives $d > 0.67$ kpc (Stairs et al. 2002). Under the assumption that general relativity provides the correct description of gravitational wave emission, the excess observed orbital period change not attributable to gravitational wave damping yields $d = 1.02 \pm 0.05$ kpc (Stairs et al. 2002). There is no statistically significant absorption evident in our pulsar spectrum along this high Galactic latitude line of sight. No previous H I absorption measurements have been made on this source.

5.4. *J1543+0929=B1541+09* (*l*=17.8°; *b*=45.8°), *Fig. 11*

No statistically significant absorption is present in this high Galactic latitude pulsar's spectrum. This is the first absorption spectrum from this pulsar.

5.5. *J2305+3100=B2303+30* (*l*=97.7°; *b*=−26.7°), *Fig. 12*

The broad, shallow dip in the displayed spectrum disappears in one of our two orthogonal polarizations, leading us to conclude that it is not real. This pulsar was also observed in 1976–1977 by Dickey et al. (1981). In that case as well, no significant absorption was seen. The pulsar traversed $\sim$1600 AU in the intervening time.

6. CONCLUSIONS

We have determined the H I absorption spectra of eight pulsars. The three low-latitude pulsars yield kinematic distances and electron densities in the inner Galactic plane visible from Arecibo. These observations mark the completion of a two-decade effort to accurately measure the H I absorption spectrum of all such pulsars that are strong enough to be accessible to this technique. Therefore, we have combined our new measurements with all others in this direction to study the electron density in this region. We find that the mean electron density in the plane in the interarm range $48° < l < 70°$ is $0.017^{+0.012}_{-0.007}$ (68% c.l.) cm^{-3}, which is $0.75^{+0.49}_{-0.22}$ (68% c.l.) of the Cordes & Lazio (2002) model value currently used by most researchers. At the lower longitudes accessible to Arecibo ($30° < l < 48°$), the Cordes & Lazio (2002) model appears to conform generally to the measurements, aside from expected local variations.

As part of the process, we show how to modify kinematic distances and electron densities as a function of the Galactic constants R_0 and Θ_0. We review recent efforts to determine the values of these constants and select the best current answers. Applying all of these results to the relativistic binary pulsar B1913+16, we find a dispersion measure distance of $d = (10.0 \pm 3.2)(R_0/8.5\ \mathrm{kpc})$ kpc, or $d = 9.0 \pm 3$ kpc if we adopt our current best choice for R_0 (Eisenhauer et al. 2005).

The five high-latitude pulsars are most useful in multiepoch studies of small-scale structure in the interstellar medium. Two were observed for the first time by us in this experiment. Of the other three, two showed no measurable absorption at either of two epochs separated by 22 yr, while one, PSR B0301+19, exhibited a significant change in absorption profile over that timespan, indicating H I structure on a $\sim$500 AU scale.

J. M. W., A. H., and A. F. were supported by grant AST 04-06832 from the National Science Foundation.

REFERENCES

Ables, J. G., & Manchester, R. N. 1976, A&A, 50, 177
Arnal, E. M., Bajaja, E., Larrarte, J. J., Morras, R., & Pöppel, W. G. L. 2000, A&AS, 142, 35
Bajaja, E., Arnal, E. M., Larrarte, J. J., Morras, R., Pöppel, W. G. L., & Kalberla, P. M. W. 2005, A&A, 440, 767
Blair, W. P., Fesen, R. A., Rull, T. R., & Kirshner, R. P. 1984, ApJ, 282, 161
Brisken, W. F., Benson, J. M., Goss, W. M., & Thorsett, S. E. 2002, ApJ, 571, 906
Brisken, W. F., Fruchter, A. S., Goss, W. M., Herrnstein, R. S., & Thorsett, S. E. 2003, AJ, 126, 3090
Burton, W. B. 1970, A&AS, 2, 291
Caswell, J. L., Murray, J. D., Roger, R. S., Cole, D. J., & Cooke, D. J. 1975, A&A, 45, 239
Chatterjee, S., Cordes, J. M., Vlemmings, W. H. T., Arzoumanian, Z., Goss, W. M., & Lazio, T. J. W. 2004, ApJ, 604, 339

Colgan, S. W. J., Salpeter, E. E., & Terzian, Y. 1988, ApJ, 328, 275
Cordes, J. M., & Lazio, T. J. W. 2002, preprint (astro-ph/0207156)
Damour, T., & Taylor, J. H. 1991, ApJ, 366, 501
Dickey, J. M., Kulkarni, S. R., Heiles, C. E., & van Gorkom, J. H. 1983, ApJS, 53, 591
Dickey, J. M., Weisberg, J. M., Rankin, J. M., & Boriakoff, V. 1981, A&A, 101, 332
Eisenhauer, F., et al. 2005, ApJ, 628, 246
Fich, M., Blitz, L., & Stark, A. A. 1989, ApJ, 342, 272
Frail, D. A., & Weisberg, J. M. 1990, AJ, 100, 743 (FW90)
Garwood, R. W., & Dickey, J. M. 1989, ApJ, 338, 841
Hartmann, D., & Burton, W. B. 1997, Atlas of Galactic Neutral Hydrogen (Cambridge: Cambridge Univ. Press)
Haslam, C. G. T., Salter, C. J., Stoffel, H., & Wilson, W. E. 1982, A&AS, 47, 1
Heiles, C. 1997, ApJ, 481, 193
Jenet, F. A., & Anderson, S. B. 1998, PASP, 110, 1467
Jenet, F. A., Anderson, S. B., & Prince, T. A. 2001, ApJ, 558, 302
Johnston, S., Koribalski, B., Wilson, W., & Walker, M. 2003, MNRAS, 341, 941
Kalberla, P. M. W., Burton, W. B., Hartmann, D., Arnal, E. M., Bajaja, E., Morras, R., & Poppel, W. G. L. 2005, A&A, 440, 775
Kerr, F. J., & Lynden-Bell, D. 1986, MNRAS, 221, 1023
Konacki, M., Wolszczan, A., & Stairs, I. H. 2003, ApJ, 589, 495
Lu, F. J., Aschenbach, B., & Song, L. M. 2001, A&A, 370, 570
Lu, F. J., Wang, Q. D., Aschenbach, B., Durouchoux, P., & Song, L. M. 2002, ApJ, 568, L49
Lyne, A. G., Anderson, B., & Salter, M. J. 1982, MNRAS, 201, 503
Manchester, R. N., Hobbs, G. B., Teoh, A., & Hobbs, M. 2005, AJ, 129, 1993
Nishiyama, S., et al. 2006, ApJ, 647, 1093
Reid, M. J., & Brunthaler, A. 2004, ApJ, 616, 872
Rosino, L., Ortolani, S., Barbuy, B., & Bica, E. 1997, MNRAS, 289, 745
Stairs, I. H., Thorsett, S. E., Taylor, J. H., & Wolszczan, A. 2002, ApJ, 581, 501
Stanimirović, S., Weisberg, J. M., Dickey, J. M., de la Fuente, A., Devine, K., Hedden, A., & Anderson, S. B. 2003a, ApJ, 592, 953
Stanimirović, S., Weisberg, J. M., Hedden, A., Devine, K. E., & Green, J. T. 2003b, ApJ, 598, L23
Taylor, J. H., & Weisberg, J. M. 1989, ApJ, 345, 434
Velusamy, T., & Becker, R. H. 1988, AJ, 95, 1162
Weisberg, J. M. 1978, Ph.D. thesis, Univ. Iowa
Weisberg, J. M., Boriakoff, V., & Rankin, J. 1979, A&A, 77, 204
Weisberg, J. M., Rankin, J. M., & Boriakoff, V. 1987, A&A, 186, 307
Weisberg, J. M., Siegel, M. H., Frail, D. A., & Johnston, S. 1995, ApJ, 447, 204
Weisberg, J. M., & Taylor, J. H. 2003, in ASP Conf. Ser. 302, Radio Pulsars, ed. M. Bailes, D. J. Nice, & S. E. Thorsett (San Francisco: ASP), 93
———. 2005, in ASP Conf. Ser. 328, Binary Radio Pulsars, ed. F. A. Rasio & I. H. Stairs (San Francisco: ASP), 25